

Constrained mixture modeling affects material parameter identification from planar biaxial tests

Lauranne Maes^{a,*}, Heleen Fehervary^a, Julie Vastmans^a, S. Jamaledin Mousavi^b, Stéphane Avril^b, Nele Famaey^a

^a*Biomechanics Section, Mechanical Engineering Department, KU Leuven, Leuven, Belgium*

^b*Mines Saint-Etienne, Univ Lyon, Univ Jean Monnet, INSERM, U 1059 Sainbiose, Centre CIS, F - 42023 Saint-Etienne, France*

Abstract

The constrained mixture theory is an elegant way to incorporate the phenomenon of residual stresses in patient-specific finite element models of arteries. This theory assumes an *in vivo* reference geometry, obtained from medical imaging, and constituent-specific deposition stretches in the assumed reference state. It allows to model residual stresses and prestretches in arteries without the need for a stress-free reference configuration, most often unknown in patient-specific modeling.

A finite element (FE) model requires material parameters, which are classically obtained by fitting the constitutive model to experimental data. The characterization of arterial tissue is often based on planar biaxial test data, to which nonlinear elastic fiber-reinforced material parameters are fitted. However, the introduction of the constrained mixture theory requires an adapted approach to parameter fitting. Therefore, we introduce an iterative fitting method, alternating between nonlinear least squares parameter optimization and an FE prestressing algorithm to obtain the correct constrained mixture material state during the mechanical test.

We verify the method based on numerically constructed planar biaxial test data sets, containing ground truth sets of material parameters. The results show

*Corresponding author: lauranne.maes@kuleuven.be, KU Leuven, Biomechanics Section, Celestijnenlaan 300 - box 2419, 3001 Leuven (Belgium)

that the method converges to the correct parameter sets in just a few iterations. Next, the iterative fitting approach is applied to planar biaxial test data of ovine pulmonary artery tissue. The obtained results demonstrate a convergence towards constrained mixture compatible parameters, which differ significantly from classically obtained parameters.

We show that this new modeling approach yields *in vivo* wall stresses similar to when using classically obtained parameters. However, due to the numerous advantages of constrained mixture modeling, our fitting method is relevant to obtain compatible material parameters, that may not be confused with parameters obtained in a classical way.

Key words: constrained mixture, deposition stretches, arterial tissue, constitutive modeling, parameter estimation

1. Introduction

1.1. Presence of residual stresses

In its *in vivo* state, an arterial segment is subjected to two kinds of external loading. The inner blood pressure, fluctuating between diastole and systole, causes a load in the radial direction. Secondly, axial stretching during growth causes axial loading. Therefore, a shortening of the segment can be observed during excision, revealing the presence of axial prestretch [1]. This excised, cylindrical configuration is freed from both types of external loads and is further referred to as the load-free configuration.

Bergel [2] discovered an uncoiling of the cylindrical configuration of an arterial segment after a radial cut. This suggested that residual circumferential stresses reside inside the load-free configuration [3, 4].

Chuong and Fung [5] found that the residual stresses homogenize the circumferential stress across the wall in its physiological condition. Rachev and Greenwald [6] hypothesized that residual stresses lead to an optimal load bearing performance, enabling to comply with blood pressure alterations. This shows

the importance of understanding and incorporating the phenomenon of residual stresses in computational models.

1.2. *Measuring residual stresses*

20 The radially cut configuration is most often considered to be stress-free [7]. After making a radial cut, an opening angle can be observed. In many cases, this angle is used as a measure for circumferential residual stresses as done by, e.g. Vaishnav and Vossoughi [8], Liu and Fung [7], Hong *et al.* [9] and Matsumoto *et al.* [10]. However, Vossoughi *et al.* [11] gave evidence that a single radial
25 cut cannot relieve the material from all stresses. Their studies show that the different layers in the arterial wall have different opening angles, such that more cuts are needed to further release the stresses. Therefore, the assumption of a radially cut stress-free state is inaccurate. Moreover, obtaining the opening angle as a measure for residual stresses is tedious work, requiring the excision
30 of a segment of the artery of interest.

1.3. *Classical modeling of residual stresses*

Classical modeling frameworks and numerical simulations with arterial tissue require the knowledge of a stress-free reference state, to which all other configurations can be related with a deformation gradient. Multiple research groups
35 have used the concept of the opening angle to define this stress-free reference state. Analytical solutions that relate the intact load-free state to the opened stress-free state have been derived by Chuong and Fung [4] by assuming plane strain deformation. Taber and Eggers [12] considered a deformation where the wall thickness is constant and the neutral line is located at the middle. Holzapfel
40 *et al.* [13] and Rachev and Greenwald [6] considered a hyperelastic, incompressible material, deforming by pure bending. An extension of this opening angle method for multiple layers was developed by Taber and Humphrey [14]. Using the same assumption of a stress-free reference state, a number of numerical simulations were carried out, starting from the opened geometry. The load-free,

45 intact geometry is then obtained by nodal displacement, as e.g. done by Gasser
et al. [15], Raghavan *et al.* [16], Balzani *et al.* [17] and Famaey *et al.* [18].

There are a number of problems associated with this approach in the case
of patient-specific modeling. The opening angle of an artery cannot be ob-
tained nondestructively. Moreover, only cylindrical geometries can be consid-
50 ered, whereas true arteries may deviate strongly from this regular shape, espe-
cially when one is interested in diseased vessels or aneurysms.

1.4. Inverse methods

As a solution, a number of groups have developed prestressing algorithms,
designed to obtain a realistic stress-state. These algorithms are based on a
55 known physiologically relevant internal pressure and pressurized geometry, that
can be obtained noninvasively through medical imaging. De Putter *et al.* [19]
and Weisbecker *et al.* [20] computed the prestressing deformation gradient, i.e.
the deformation gradient relating the known *in vivo* geometry to the load-free
geometry, with a backwards incremental method. At each iteration, the re-
60 quired pressure incrementation is mapped to the deformation needed to relate
the known *in vivo* geometry to the current estimate of the load-free geome-
try, leading to an equilibrium between the *in vivo* geometry and pressure after
convergence in the last increment.

An alternative approach was developed by Bols *et al.* [21], who proposed a
65 backwards displacement method. At each iteration, the *in vivo* pressure is ap-
plied to the approximated load-free configuration. Subsequently, the resulting
nodal displacement is subtracted from the known *in vivo* geometry. After con-
vergence, a solution for a stress-free state is obtained, which can be pressurized
to determine any physiological configuration of the artery.

70 Other prestressing algorithms were described by Raghavan *et al.* [22] and
Gee *et al.* [23, 24]. These algorithms allow the integration of prestress at diastole
in finite element (FE) models, greatly enhancing the reliability of simulations of
patient-specific cases. However, all previously mentioned algorithms are unable
to reliably represent circumferential residual stresses in arterial tissue, because

75 the application to cylindrical geometries yields a stress-free zero-pressure configuration [19, 20].

1.5. Constrained mixture modeling

The aforementioned algorithms assume that, while deforming together in the arterial wall, the different material constituents experience the same stretch levels. However, residual stresses likely originate from the fact that the constituents
80 are deposited at different time points and experience different levels of stretch during multiple events of growth and remodeling [25, 26, 27]. Therefore, a new theoretical framework was proposed by Bellini *et al.* [28], based on the constrained mixture theory, first described by Humphrey and Rajagopal [29]. This
85 framework accounts for the natural stress state of the individual constituents with constituent-specific deposition stretches, relating an *in vivo* reference configuration to the individual rest lengths of the constituents. Results show a reliable prediction of the zero-pressure configuration and the residual stresses, without the need of an opening angle or a stress-free reference configuration.

90 Moreover, the constrained mixture theory is increasingly used in the modeling of growth and remodeling in soft tissues, as done by [30, 31, 32, 33, 34, 35, 36, 37]. *In vivo*, these remodeling processes occur through mass turnover of the different constituents [29]. Due to the microstructurally motivated nature of the constrained mixture theory, it offers a relevant framework for growth and
95 remodeling algorithms.

The above modeling approach implies knowledge of the material parameters. This can be obtained, e.g. from planar biaxial tests, or from extension-inflation tests. However, the classical approaches to the parameter fitting of planar biaxial test data does not take the concept of residual stresses into account. They
100 assume a stress-free configuration at the start of the test and a homogeneous stretch state of the material. On the other hand, the constrained mixture approach assumes a relevant *in vivo* reference state. We hypothesize that this assumption has an important influence on the resulting material parameters and propose an original solution to incorporate the constrained mixture modeling

105 approach and accompanying deposition stretches into the parameter estimation process.

Therefore, we introduce an iterative parameter fitting approach, alternating between a nonlinear least squares optimization and a prestressing FE simulation. This new approach allows to determine material parameters compatible with the
 110 constrained mixture theory, enabling a more biologically relevant approach for the modeling of healthy, matured arteries. In the present work, this framework is verified against numerically constructed planar biaxial data sets and tested on real experimental data, as explained in the following sections.

2. Material and Methods

115 The description of the method starts with a depiction of the considered material model. Subsequently, we explain how deposition stretches for the constrained mixture model are obtained and how they are integrated in the parameter fitting on planar biaxial test data. Finally, an explanation of the verification and testing approach is given.

120 2.1. Material description

An anisotropic, hyperelastic description of the artery's mechanical behavior can be made through an additive decomposition of a strain energy density function Ψ , with a contribution of the isotropic extracellular matrix material, mainly elastin, and the embedded collagen fibers, which are assumed to run along two preferred directions. This leads to the classic Gasser-Ogden-Holzapfel (GOH) formulation [38]

$$\Psi = C_{10}(I_{1,e} - 3) + \frac{k_1}{2k_2} \sum_{i=4,6} \left\{ \exp \left\{ k_2 [(\kappa I_{1,c} + (1 - 3\kappa)I_{i,c}) - 1]^2 \right\} - 1 \right\}, \quad i = 4, 6, \quad (1)$$

with C_{10} , k_1 , k_2 and κ material constants. $I_{1,e}$ and $I_{1,c}$ are the first invariants of the right Cauchy-Green stretch tensors \mathbf{C}_e and \mathbf{C}_c , applied to the elastin and the collagen constituents, respectively. $I_{i,c}$ is a pseudo-invariant of \mathbf{C}_c , and

represents the stretch along each preferred fiber direction as

$$I_{i,c} = \mathbf{M}_i \cdot (\mathbf{C}_c \mathbf{M}_i), \quad i = 4, 6, \quad (2)$$

with $\mathbf{M}_i = [0 \ \cos \alpha_i \ \sin \alpha_i]$ the undeformed fiber orientation vector, where the order of the axes is given as r (radial), θ (circumferential) and z (axial). α_i is the mean angle of the fibers with respect to the circumferential direction of the artery in the θ, z -plane.

Note that in a classical modeling approach,

$$\mathbf{C}_e = \mathbf{C}_c = \mathbf{C} = \mathbf{F}^T \mathbf{F}, \quad (3)$$

where \mathbf{F} is the total deformation gradient with respect to a stress-free reference geometry. Contrarily, in the constrained mixture theory,

$$\mathbf{C}_j = \mathbf{F}_j^T \mathbf{F}_j \quad j = e, c, \quad (4)$$

where

$$\mathbf{F}_j = \mathbf{F} \mathbf{G}_j \quad j = e, c, \quad (5)$$

125 with \mathbf{F} the total deformation gradient of the mixture with respect to an *in vivo*, diastolic reference state and \mathbf{G}_j the deposition stretch tensor of elastin or collagen, respectively. Note also that all considered deformations are fully isochoric, such that no volumetric energy contribution is considered.

Two layers through the thickness of the arterial wall are considered with
 130 different material properties, corresponding to the media and the adventitia respectively. Bellini *et al.* [28] considered that most arterial elastin is located in the media. Therefore, the assumption is made that C_{10} is ten times higher in the media. The stiffness k_1 and strain-stiffening k_2 of the collagen fibers are considered equal in both layers. These fibers are more aligned with the
 135 circumferential direction in the media than in the adventitia [39], such that α is assumed to be zero for both fiber families in the media. The fiber dispersion, represented by κ is assumed to be the same in both layers of the arterial wall. In total, there are five independent parameters, the medial $C_{10,M}$, the fiber

parameters k_1 , k_2 and κ and the adventitial fiber angle α_A with respect to the circumferential direction. The used parameters are summarized in table 1.

Media (M)	Adventitia (A)
$C_{10,M}$	$C_{10,A} = 0.1 \cdot C_{10,M}$
$k_{1,M} = k_1$	$k_{1,A} = k_1$
$k_{2,M} = k_2$	$k_{2,A} = k_2$
$\kappa_M = \kappa$	$\kappa_A = \kappa$
$\alpha_M = 0$	α_A

Table 1: Adventitial and medial material parameters.

2.2. An algorithm to find deposition stretches

According to Bellini *et al.* [28], the constituents in the diastolic reference configuration of the artery experience different prestretches. These stretches are introduced through deposition stretch tensors \mathbf{G}_e and \mathbf{G}_c for elastin and collagen respectively. These deformation gradients are defined in accordance with [30] and as described below. Collagen fibers may have a fast turnover rate and are deposited at a preferred stretch state [29]. Therefore, we assume a constant and known deposition stretch g_c for collagen along the fiber direction [28, 30, 40], justified by the fact that we focus on healthy matured arteries. An approximate value of collagen prestretch of 1.1 was found by Bellini *et al.* [28] and used in the methods explained further on. For a certain fiber family with orientation vector \mathbf{M} , \mathbf{G}_c may then be written as [32]

$$\mathbf{G}_c = g_c \mathbf{M} \otimes \mathbf{M} + \frac{1}{\sqrt{g_c}} (\mathbf{I} - \mathbf{M} \otimes \mathbf{M}), \quad (6)$$

where \mathbf{I} is the identity tensor.

On the other hand, elastin is deposited at an early stage of development and is very stable. As a consequence, it is stretched during growth. \mathbf{G}_e therefore varies from material point to material point and balances out the reference diastolic configuration and corresponding pressure. Considering a known and constant axial deposition stretch $g_{e,ax}$ and an isochoric deformation, the solution is unique.

The unknown deposition stretch values are determined iteratively, similarly to [30] and [40]. A finite element (FE) method, schematically represented in figure 1, is implemented by initially considering a load- and stress-free diastolic configuration. In a first step, the diastolic pressure is applied to the geometry, while \mathbf{G}_c and an initial elastin deposition stretch tensor

$$\mathbf{G}_e = \begin{bmatrix} \frac{1}{\sqrt{g_{e,ax}}} & 0 & 0 \\ 0 & \frac{1}{\sqrt{g_{e,ax}}} & 0 \\ 0 & 0 & g_{e,ax} \end{bmatrix} \quad (7)$$

are applied to the material, where $g_{e,ax}$ represents the axial deposition stretch
150 of elastin.

In all following simulation steps, the resulting deformation gradient with respect to the diastolic reference state in each material point is multiplied to the existing \mathbf{G}_e , from which the shear terms are removed, to cause an apparent stiffening and recoiling towards the reference configuration. This is repeated
155 until the current configuration matches the initial configuration, i.e. when the average absolute nodal displacement is below a threshold defined as 1% of the diastolic wall thickness [40]. In practice, the algorithm is run using a user material subroutine (UMAT) in Abaqus/Standard 2017 (Dassault Systèmes Simulia Corp., Providence Rhode Island, USA). See the appendix for further details on
160 the implementation. This algorithm is further referred to as the ‘prestressing algorithm’.

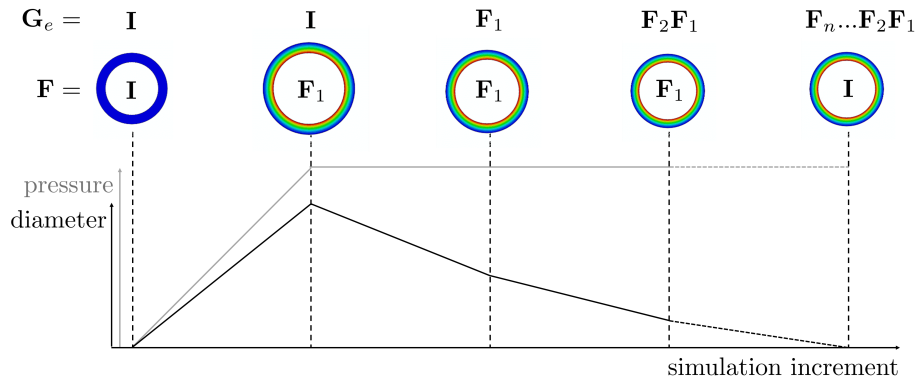


Figure 1: Schematic representation of the prestressing algorithm to obtain the elastin deposition stretches. \mathbf{G}_e is the deformation gradient accounting for the elastin deposition stretch and \mathbf{F} is the deformation of the artery with respect to its diastolic reference configuration. Adapted from [30].

2.3. Parameter fitting of planar biaxial tests

2.3.1. Classical approach

During a planar biaxial test, a flat squared sample of material is attached at
 165 its four sides to the actuators of the testing machine. This way, the displacement
 in two perpendicular directions can be applied independently. The normal forces
 applied by the actuators can be measured directly and are further referred to as
 the experimental forces, f_{ii}^{exp} , with i indicating one of the two test directions.
 The deformation of the sample is usually obtained through image processing,
 170 where four markers or a speckle pattern in the central region of the sample are
 tracked, from which the in-plane deformation gradient can be derived.

The obtained deformation gradient \mathbf{F} at each sampling time point of the
 experiment is used to estimate the required first Piola-Kirchhoff stress as

$$\mathbf{P}^{mod} = J \boldsymbol{\sigma}^{mod} \mathbf{F}^T, \quad (8)$$

with $\boldsymbol{\sigma}^{mod}$ the Cauchy stress calculated as

$$\boldsymbol{\sigma}^{mod} = \frac{1}{J} \frac{\partial \Psi}{\partial \mathbf{F}} \mathbf{F}^T - p \mathbf{I}. \quad (9)$$

Here, \mathbf{F} pertains to the total deformation during the biaxial test and $J = \det(\mathbf{F})$. Ψ is the strain energy density function of the material as described in equation 1, with a currently unknown set of material parameters $\mathbf{p} = [C_{10,M}, k_1, k_2, \kappa, \alpha_A]$. The hydrostatic pressure p multiplied with the identity tensor \mathbf{I} arises from a constraint of incompressibility and is calculated by assuming a zero out-of-plane stress. The first Piola-Kirchhoff stress is then transformed to the model force by multiplication with a reference surface as

$$f_{ij}^{mod} = P_{ij}A_j \quad i, j = 1, 3, \quad (10)$$

where f_{ij} is the force along the i -th direction, acting on the j -th surface, and A_j the undeformed surface upon which the force is acting.

To obtain the unknown material parameters, the following objective function is minimized:

$$\min_{\mathbf{p}} \sum_{j=1}^n \left[(f_{11}^{mod}(t_j) - f_{11}^{exp}(t_j))^2 + (f_{22}^{mod}(t_j) - f_{22}^{exp}(t_j))^2 \right], \quad (11)$$

with t_j the sampling time points of the experiment and $f_{ii}^{exp}(t_j)$ the experimen-
 175 tially measured force. In the experiments that follow, we used a nonlinear least squares optimization routine *lsqnonlin* in Matlab 2017a (The Mathworks Inc., Natick, Massachusetts, USA), along with the *multistart* function with 10 initial parameter sets in order to obtain the global minimum.

In the classical biaxial fitting approach, no deposition stretches are modeled,
 180 and all constituents of the mixture are assumed to feel the same deformation gradient $\mathbf{F} = \mathbf{F}_{biax}$. As such, the configuration at the beginning of the biaxial test is assumed to be the stress-free reference configuration.

2.3.2. Constrained mixture-compatible fitting

Considering diastole to be the reference configuration, a testing sample pre-
 185 pared for a biaxial test has undergone depressurization, release of axial pre-stretch $\mathbf{F}_{release}$, opening to release circumferential stresses and further flattening to a square patch $\mathbf{F}_{flatten}$. Considering also the deposition stretches of collagen and elastin that were present at diastole, it is highly unlikely that the

constituents are stress-free at the start of the biaxial test. Rather, during the
 190 biaxial test, they will have the following deformation:

$$\mathbf{F}_j = \mathbf{F}_{biax} \mathbf{F}_{flatten} \mathbf{F}_{release} \mathbf{G}_j, \quad j = e, c. \quad (12)$$

Hence, when calculating the Cauchy stresses to obtain the model forces in the objective function of equation 11, this total deformation for each of the constituents should be taken into account, i.e.

$$\boldsymbol{\sigma}^{mod} = \frac{1}{J} \frac{\partial \Psi}{\partial \mathbf{F}} \mathbf{F}^T - p \mathbf{I} = \frac{1}{J} \left(\frac{\partial \Psi}{\partial \mathbf{F}_e} : \frac{\partial \mathbf{F}_e}{\partial \mathbf{F}} + \frac{\partial \Psi}{\partial \mathbf{F}_c} : \frac{\partial \mathbf{F}_c}{\partial \mathbf{F}} \right) \mathbf{F}^T - p \mathbf{I}. \quad (13)$$

Note however, that the deposition stretch tensors as well as the deformations due to depressurization, release of axial prestretch, opening and flattening depend on the geometry and material properties of the tested sample, the latter being exactly what we are trying to optimize. Hence, an iterative scheme
 195 is proposed to obtain these constrained mixture-compatible (CMC) material parameters, as shown in figure 2 and described below.

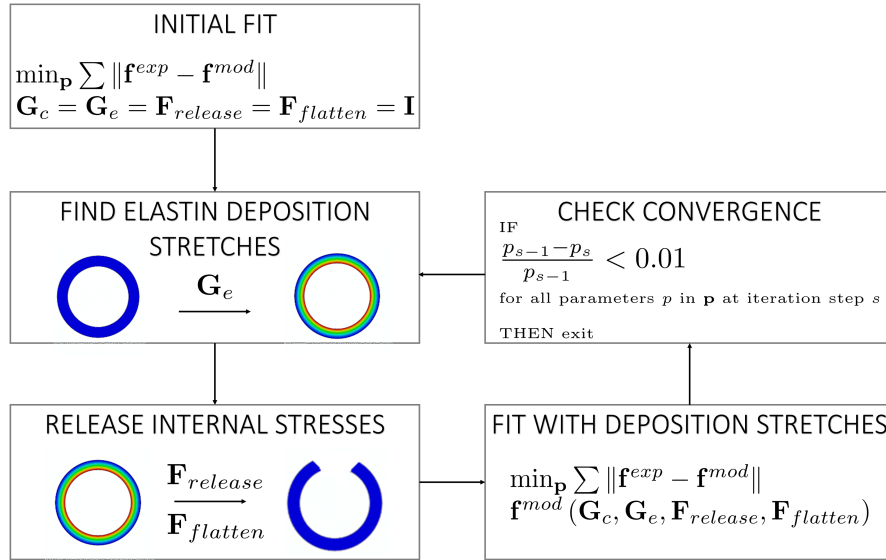


Figure 2: Schematic representation of the iterative parameter fitting approach, compatible with the constrained mixture theory.

In the initialization step, a classical parameter fitting scheme as described in section 2.3.1 is applied, yielding a set of material parameters. These parameters are then used in the prestressing algorithm, described in section 2.2, to
 200 obtain accompanying deposition stretches. At the end of the algorithm, the resulting pressurized artery is depressurized and axial stresses are released. The resulting deformation gradient is stored as $\mathbf{F}_{release}$. Next, a radial cut is made through the mesh to release the residual circumferential stresses. The resulting deformation in this last step is assigned to $\mathbf{F}_{flatten}$, assuming that the circum-
 205 ferential stretches from this nearly stress-free configuration to a flat unloaded configuration are negligible.

Now that estimates of $\mathbf{F}_{flatten}$, $\mathbf{F}_{release}$, \mathbf{G}_e and \mathbf{G}_c are available, a new parameter fitting procedure is performed, where this time the model stresses are calculated as in equation 13. It is important to note that $\mathbf{F}_{flatten}$, $\mathbf{F}_{release}$ and \mathbf{G}_e are not constant through the thickness of the artery. Therefore, the stress field of the biaxial sample is not homogeneous through the thickness and multiple material layers must be considered during the parameter fitting. One average deposition stretch tensor \mathbf{G}_e per layer of finite elements is extracted from the simulation. The combined deformation gradient $\mathbf{F}_{flatten}\mathbf{F}_{release}$ is determined at the end of the mentioned simulations with respect to the initial diastolic configuration. The axial shortening is extracted and an average circumferential stretch per layer is determined from the total change in length of these element edges. This results in an overall axial stretch λ_z and one circumferential stretch λ_θ per element layer. Considering an isochoric deformation, $\mathbf{F}_{flatten}\mathbf{F}_{release}$ is then written as

$$\mathbf{F}_{flatten}\mathbf{F}_{release} = \begin{bmatrix} \frac{1}{\lambda_\theta\lambda_z} & 0 & 0 \\ 0 & \lambda_\theta & 0 \\ 0 & 0 & \lambda_z \end{bmatrix}. \quad (14)$$

The model force is calculated at each layer as explained above and these are summed to obtain an overall model force to be matched to the experimentally measured forces. With the newly obtained material parameters, the prestressing
 210 algorithm is rerun, followed by the calculation of $\mathbf{F}_{release}$ and $\mathbf{F}_{flatten}$. This

loop is repeated until convergence of the material parameters, i.e. until the relative difference between subsequent parameters is smaller than 1% for each of the five independent fitted parameters.

2.4. Verification study

215 The constrained mixture-compatible (CMC) parameter fitting approach described above is verified against numerically constructed biaxial test data. This verification study is based on six sets of ground truth parameters, given in table 2. The five independent parameters are given. The elastin stiffness in the media $C_{10,M}$ is considered ten times higher than the elastin stiffness in the adventitia
 220 and the fibers are considered to run approximately in the circumferential direction in the media, whereas the fiber angle in the adventitia α_A can be different from zero.

set	$C_{10,M}$ [MPa]	k_1 [MPa]	k_2 [-]	κ [-]	α_A [rad]	$g_{e,ax}$ [-]	g_c [-]
1	0.5	0.1	10.0	0.2	0.7	1.1	1.05
2	0.2	0.5	2.0	0.2	0.7	1.1	1.05
3	0.5	0.1	10.0	0.0	1.2	1.1	1.05
4	0.5	0.1	10.0	0.2	0.7	1.3	1.1
5	0.2	0.05	10.0	0.2	0.7	1.3	1.1
6	0.2	0.05	10.0	0.0	1.2	1.1	1.05

Table 2: The six sets of material parameters used in the verification study for the CMC parameter fitting, with corresponding axial elastin deposition stretch $g_{e,ax}$ and collagen deposition stretch g_c .

These parameter sets are used in FE simulations in Abaqus. The diastolic geometry of a human thoracic aorta is modeled as a cylinder with an inner
 225 radius of 15.0 mm. The media and adventitia thicknesses are 1.18 mm and 0.93 mm respectively [39]. Due to symmetry of the problem, only half of the cylinder is modeled in Abaqus and symmetry boundary conditions are assigned at the appropriate symmetry plane. The mesh contains 12096 hexahedral, fully integrated, hybrid elements (C3D8H). The total of four medial and four adven-

230 titial element layers ensures mesh convergence. The axial planes are fixed and
a diastolic pressure of 10 kPa is applied to the inner surface of the cylinder. All
deposition stretches are determined as explained in section 2.2. $\mathbf{F}_{release}$ and
 $\mathbf{F}_{flatten}$ are obtained as in section 2.3.2.

A second simulation starts from a cuboid geometry, composed out of 512
235 C3D8H elements with a total of eight element layers, representing the arterial
test sample at the beginning of a biaxial test. The thickness is set according to
the resulting thickness after the simulation of the radial cut. The same material
properties are assigned to this mesh, taking into account the difference between
the media and adventitia. In addition, all obtained layer-specific deposition
240 stretches and deformation gradients are assigned to the material, i.e. $\mathbf{F}_{release}$,
 $\mathbf{F}_{flatten}$ and \mathbf{G}_e .

An ideal biaxial test is then simulated by assigning displacement increments
in the circumferential and axial direction in three different ratios of maximal
displacement causing up to approximately 25% stretch in the two test directions,
245 i.e. 1:1, 0.5:1 and 1:0.5. Subsequently, the resulting reaction forces at the
displacement sites and the nodal coordinates of the marker nodes are extracted
at each increment, resulting in numerically constructed biaxial test data sets.
Figure 3 represents the workflow followed to obtain these data sets. Next, both
parameter fitting approaches described in section 2.3 are applied to the obtained
250 data sets. Classical material parameters are obtained in the first iteration of
the fitting approach and CMC parameters are obtained after convergence.

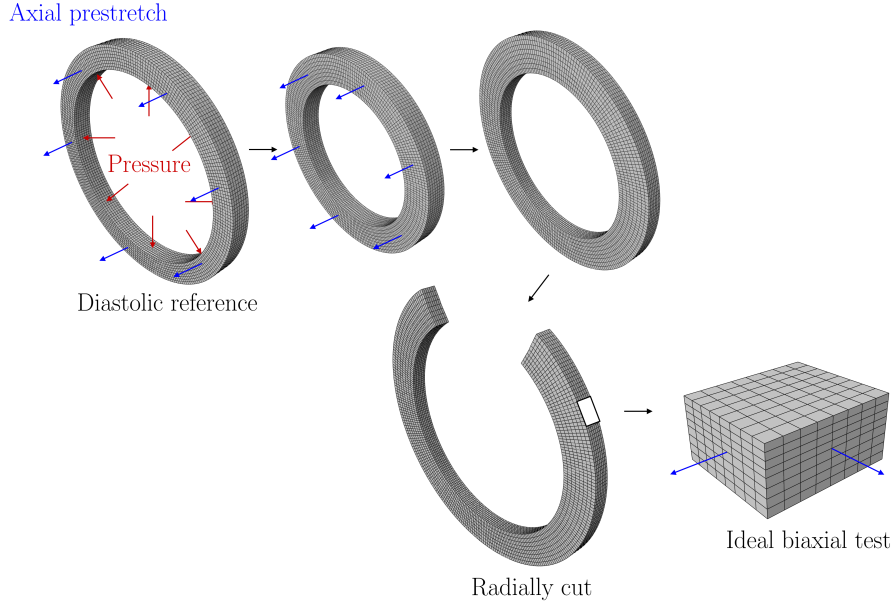


Figure 3: Schematic representation of the followed steps in the verification approach to obtain numerically constructed biaxial test data sets.

2.5. Application to experimental data

2.5.1. Parameter fitting

After verification, the CMC parameter fitting approach was applied to actual
 255 test data, obtained from Vastmans *et al.* [41]. A tissue sample of a pulmonary
 artery was subjected to a planar biaxial tensile test, where the circumferential
 and axial direction were aligned according to the two test directions. The sample
 was loaded up to 1.2 N in three different load ratios between the circumferential
 load and the axial load, i.e. 1:1, 0.5:1 and 1:0.5. More information on the
 260 harvesting and preparation of this arterial tissue sample and about the applied
 testing protocol can be found in [41] (sheep 1983, pulmonary sample 2, P1).
 During the same biaxial test, four markers were manually attached to the tissue
 and tracked, from which \mathbf{F}_{biax} is obtained at each loading point as explained in
 section 2.3.1.

265 For the CMC parameter fitting approach, an FE model of a half cylinder is built, corresponding to the geometry of the considered sheep pulmonary artery. The diameter of the artery at diastole is set to 19.4 mm, i.e. the diameter measured *in vivo* in [41]. The *ex situ* sample thickness is reported to be 3.20 mm [41]. Based on trial-and-error, the *in vivo* thickness of the artery is estimated at 270 2.50 mm. The adventitia-to-media thickness ratio is roughly estimated at one, based on findings by [42], such that each layer thickness is set to 1.25 mm in the diastolic configuration. The length of the cylinder is set to 2.0 mm.

The mesh is built out of 5136 C3D8H elements. Both the media and the adventitia contain four element layers, such that eight material layers with different deposition stretches can be identified. The total of eight layers ensure 275 mesh convergence. The same boundary conditions as in section 2.4 are applied to the model in order to obtain \mathbf{G}_e , $\mathbf{F}_{release}$ and $\mathbf{F}_{flatten}$ at each iteration of the fitting. The diastolic pulmonary blood pressure is estimated at 2 kPa [30]. The axial elastin deposition stretch $g_{e,ax}$ is set to 1.16, i.e. an approximate 280 axial prestretch obtained from unpublished results related to [41]. The collagen deposition stretch g_c is set to 1.1, a value found by [28] for mouse carotid arteries.

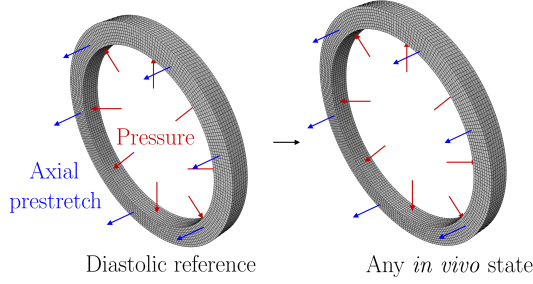
2.5.2. Comparison of the classical and constrained mixture modeling approach

A comparison of the wall stresses obtained with the constrained mixture 285 modeling approach and the classical approach for the modeling of the sheep pulmonary artery can be made after material parameters for both are obtained. The classical material parameters are obtained in the first iteration of the developed fitting approach, whereas the CMC parameters are obtained after convergence of the entire procedure. In the case of the constrained mixture approach, 290 this final parameter set is used in combination with the same FE model as in the previous section, to obtain the assumed diastolic reference state of the sheep artery according to section 2.2. In a next simulation step, the deposition stretches are kept constant and the pressure is increased to a pulmonary systolic pressure level of 3 kPa.

295 The classical modeling approach considers the radially cut configuration as
a stress-free reference state. Therefore, another FE model of the physiologically
loaded artery is built, starting from this geometry, obtained by removing the
appropriate boundary conditions after the final iteration of the CMC parameter
fitting to simulate the excision and radial cut of the artery. This *ex vivo* geom-
300 etry was approximated by a cylindrical section with a radius of 11.93 mm and
an opening angle Θ of approximately 54° , as defined in figure 4. The material
is defined by the same UMAT in Abaqus, where $\mathbf{G}_e = \mathbf{G}_c = \mathbf{I}$, in combination
with the material parameters obtained at the first iteration of the fitting proce-
dure. The initial material orientations are determined by fitting a circle through
305 the nodes of the new reference geometry in a plane perpendicular to the axial
direction, following the approach by Pratt [43]. The fibers are assumed to run
in a plane perpendicular to the radial direction obtained from the fitting of the
circle. In a first simulation step, the opening angle is closed. Subsequently, an
axial displacement of the top of the cylinder is imposed, while the bottom is
310 fixed in the axial direction, in order to restore the axial prestretch. The level of
displacement is determined based on the axial recoil that was observed earlier.
In a next step, the diastolic blood pressure is applied to the inner surface, and
is then increased to the systolic level. A schematic overview of the simulation
steps for both approaches is shown in figure 4.

315 From both simulation approaches, the Cauchy stresses in all directions at
diastole and systole are extracted. The obtained values are compared and shown
in section 3.2.2 in order to assess the similarity. Finally, both FE models are
discussed in section 4.3.

CONSTRAINED MIXTURE MODELING



CLASSICAL MODELING

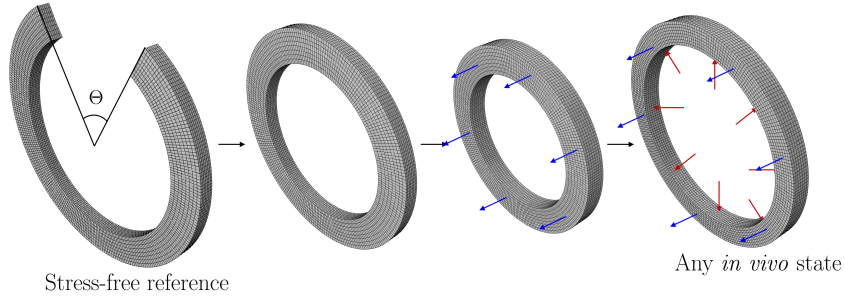


Figure 4: Schematic representation of the constrained mixture modeling approach and the classical modeling approach.

3. Results

320 3.1. Verification study

Table 3 gives an overview of the results of the verification study for the CMC parameter fitting method accounting for residual stresses. The fitted parameter sets are shown and compared to the true parameters from table 2 via the mean absolute percentage error (MAPE), computed as

$$\frac{100\%}{5} \sum_{i=1}^5 \left| \frac{p_{i,true} - p_i}{p_{i,true}} \right| \quad (15)$$

for all estimated parameters p_i and corresponding ground truth parameters $p_{i,true}$. The ‘classical’ parameters are obtained by considering a fully stress-free

test sample at the beginning of the biaxial test. These parameters are also the results of the first iteration of the CMC fitting procedure. After convergence of this procedure, the CMC parameters are obtained, after a certain required number of iterations (nb. it.). Remember that the value of $C_{10,A}$ in the adventitia is dependent on the value in the media and ten times smaller. Therefore it is not shown in the table. The fiber angle in the media is always considered zero and hence not fitted nor shown.

set		nb. it.	$C_{10,M}$ [MPa]	k_1 [MPa]	k_2 [-]	κ [-]	α_A [rad]	MAPE [%]
1	true		0.5000	0.1000	10.0000	0.2000	0.7000	
	classical		0.4999	0.0732	8.2860	0.1216	0.5949	19.6
	CMC	4	0.5000	0.1001	9.9969	0.2000	0.6999	0.03
2	true		0.2000	0.5000	2.0000	0.2000	0.7000	
	classical		0.1787	0.3323	1.7366	0.1394	0.7373	18.6
	CMC	4	0.2001	0.5003	2.0031	0.2001	0.6997	0.07
3	true		0.5000	0.1000	10.0000	0.0000	1.2000	
	classical		0.7375	0.3349	13.9997	0.0000	0.0000	84.5
	CMC	9	0.4998	0.1001	9.9994	0.0000	1.2003	0.03
4	true		0.5000	0.1000	10.0000	0.2000	0.7000	
	classical		0.5366	0.1601	10.0751	0.0590	0.0000	47.7
	CMC	8	0.4997	0.1003	9.9910	0.1998	0.6997	0.12
5	true		0.2000	0.0500	10.0000	0.2000	0.7000	
	classical		0.2092	0.0323	7.2787	0.0515	0.0000	48.3
	CMC	9	0.2000	0.0500	9.9840	0.1998	0.6997	0.06
6	true		0.2000	0.0500	10.0000	0.0000	1.2000	
	classical		0.2325	0.0110	17.6526	0.0000	0.9336	38.6
	CMC	5	0.2000	0.0500	10.0012	0.0000	1.2000	~ 0

Table 3: The results of the validation study: the true parameters, the fitted parameters with the classical approach and the CMC parameters obtained iteratively by taking into account residual stresses. The number of iterations is indicated (nb. it.) and the mean absolute average error (MAPE) of the fitted parameters, as compared to the true values.

330 Figure 5 shows how the material parameters evolve through the iterations
for parameter set number 6. The full line represents the obtained parameters
at each iteration step, which are compared to the dashed line, representing the
‘true’ parameters. The evolution of κ is not shown since it was zero at each
iteration for this parameter set. The figure reveals a clear convergence towards
335 the ‘true’ parameters after 5 iterations.

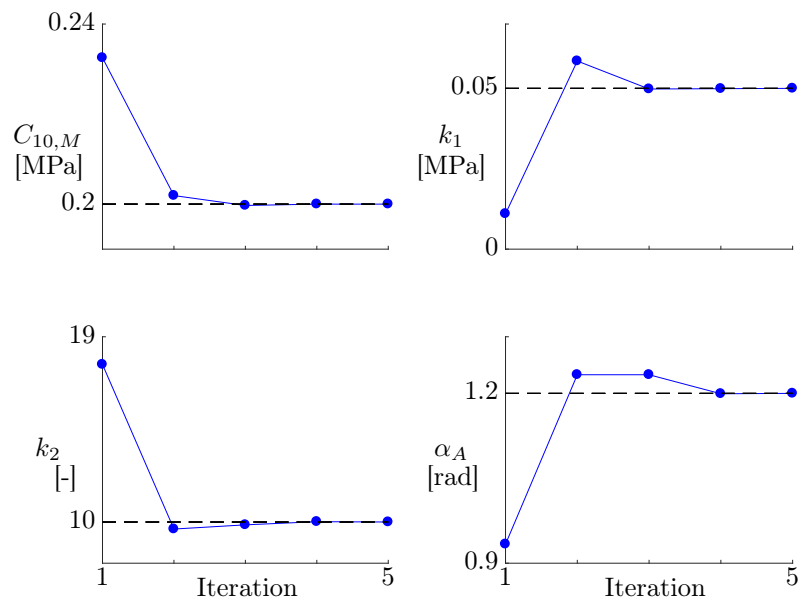


Figure 5: Evolution of the fitted material parameters during the iterative fitting approach (full line) of set number 6. Convergence towards the ‘true’ parameters (dashed line) can be observed after 5 iterations.

3.2. Application to experimental data

3.2.1. Parameter fitting

The iterative parameter fitting approach was tested on actual planar biaxial test data obtained on sheep pulmonary artery tissue. The results are given in
340 table 4. The medial stiffness parameter $C_{10,M}$ is given, as well as the fiber

parameters k_1 and k_2 , the fiber dispersion parameter κ and the adventitial fiber orientation parameter α_A , for two cases. First, these parameters are obtained after a classical fitting, based on the two-layered constitutive model, and second, after convergence of the iterative CMC fitting approach.

345 Figure 6 shows the evolution of the material parameters in function of the iteration number. Iteration number one corresponds to the initial fitting, according to the classical approach of obtaining material parameters. The fit of the model data to the experimental data at the first and last iteration is shown in figure 7. The initial fit is slightly better with a normalized root-mean-square
 350 error (NRMSE), a measure for the objective function of the optimization, of 0.1165 versus 0.1177 at the final fit.

	nb. it.	$C_{10,M}$ [MPa]	k_1 [MPa]	k_2 [-]	κ [-]	α_A [rad]	NRMSE [-]
classical		0.0115	0.0027	11.81	0.0949	0.7112	0.1165
CMC	7	0.0099	0.0126	21.31	0.2034	0.6329	0.1177

Table 4: The results of the fitting to the actual planar biaxial data from sheep pulmonary artery tissue. The classical set of parameters is obtained by assuming a stress-free reference state at the beginning of the test. The CMC set of parameters is obtained by taking into account residual stresses and an *in vivo* reference state. The required number of iterations is given, as well as the obtained parameters and the NRMSE for both fits.

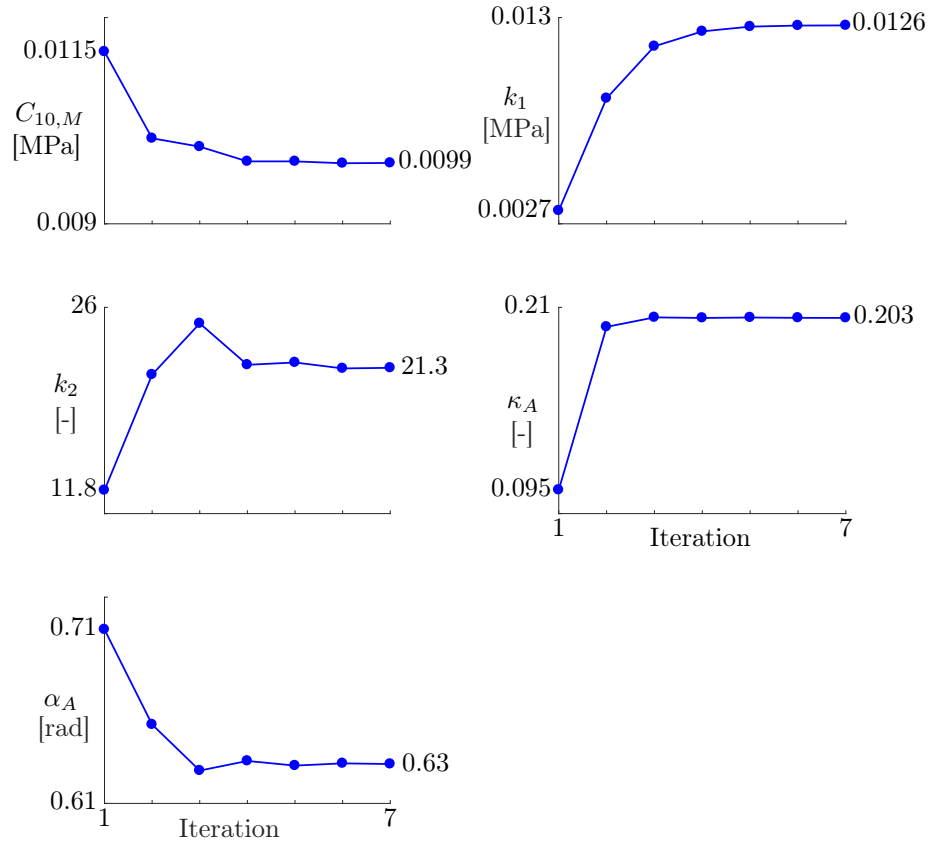


Figure 6: Evolution of the fitted material parameters during the iterative CMC approach applied to planar biaxial test data from sheep pulmonary artery tissue.

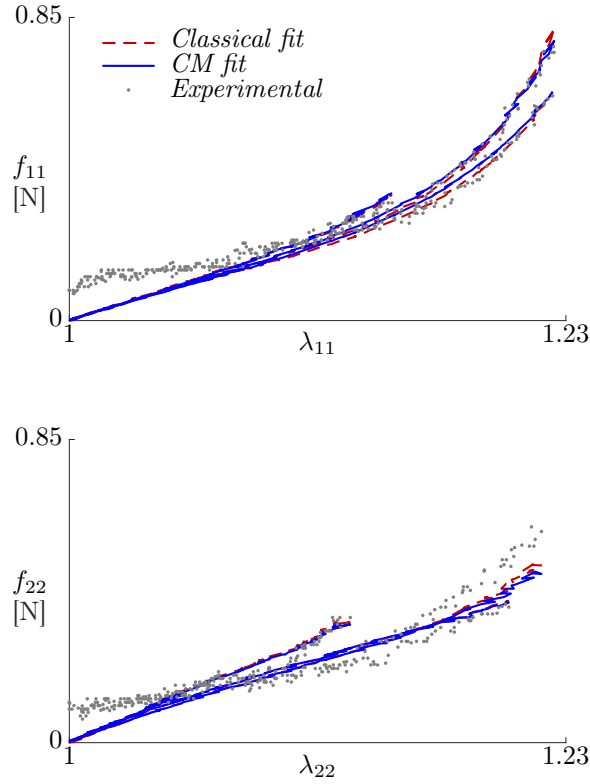


Figure 7: Comparison of the fit of the model forces to the experimental reaction force in circumferential and axial direction (f_{11} and f_{22} respectively) and the last iteration (constrained mixture, CM fit). The grey dots represent the experimental data obtained from a planar biaxial test on ovine pulmonary artery tissue, the dashed red line is the classical model data and the full blue line is the constrained mixture model data. The forces are given in function of the measured circumferential and axial stretches during the test (λ_{11} and λ_{22}) for three loading ratios between both directions.

3.2.2. Comparison of the classical and constrained mixture modeling approach

Figure 8 gives an overview of the Cauchy stresses across the thickness of the arterial wall of the considered sheep pulmonary artery. These stresses are obtained from two different modeling approaches, as explained in section 2.5.2: the constrained mixture approach and the classical, stress-free reference approach.

In both cases, the stresses are given at diastolic state as well as at systolic state.

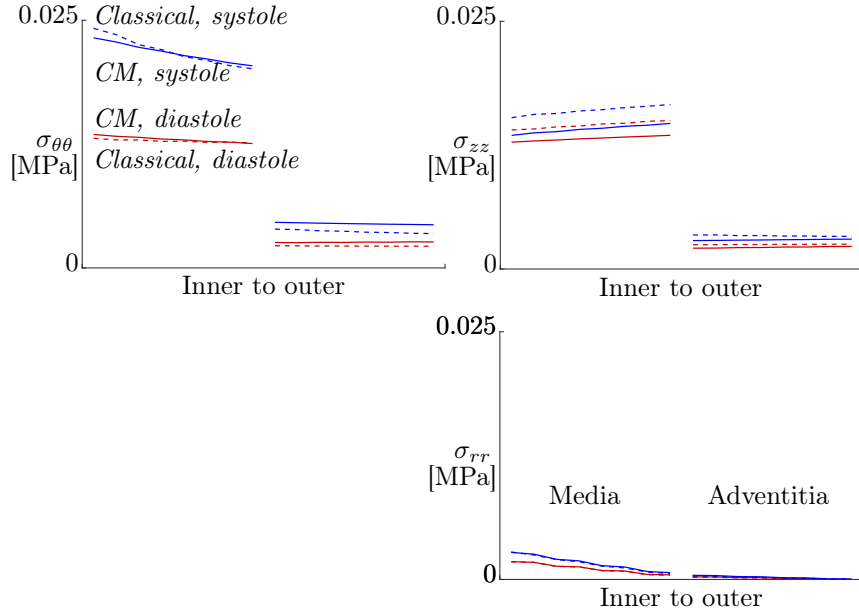


Figure 8: Comparison of the constrained mixture and classical modeling approach. The full lines represent the Cauchy stresses across the thickness of the wall for the constrained mixture approach. The dashed lines represent the same stresses obtained with the classical modeling approach. Stresses are shown at diastole and systole, i.e. an inner pressure of 2 kPa and 3 kPa respectively. $\sigma_{\theta\theta}$, σ_{zz} and σ_{rr} represent the circumferential, axial and radial Cauchy stresses.

4. Discussion

The objective of this study was to investigate how material parameters for
 360 arterial tissue are affected by the introduction of the constrained mixture mod-
 eling approach. An efficient method able to provide these parameters based on
 planar biaxial test data was introduced, addressing the need for reliable mate-
 rial parameters to be used in e.g. growth and remodeling algorithms based on
 the constrained mixture theory. This method was verified and applied to ac-
 365 tual mechanical test data. Subsequently, the classical way of modeling residual

stresses and axial prestress in the arterial wall is compared to the constrained mixture modeling approach.

4.1. Verification study

Table 3 demonstrates the general performance of the CMC fitting approach and how the obtained material parameters relate to the classical parameters. 370 The method converged in less than ten iterations for the six tested cases. The error of the final parameters with respect to the ground truth parameters is an order of magnitude smaller than 1% and negligible. Therefore, the method to obtain material parameters for constrained mixture modeling performs well as 375 expected in a reasonable number of iterations for all test cases.

When comparing the ground truth and CMC material parameters to the classical parameters obtained in the first iteration step, a clear difference can be observed, although the order of magnitude for all parameters stays similar. No clear trend in the evolution from the classical set to the final set can be 380 noted. In four of six tested cases, the initial matrix stiffness $C_{10,M}$ is bigger at the first iteration than at the final one. In the two other cases, the value of this stiffness parameter increases. Figure 5 shows that the evolution of the material parameters over the iterations is not necessarily steady. For example, for parameter set number six, an overshoot can be observed at the second it- 385 eration for parameters k_1 , k_2 and α_A , whereafter the parameters evolve in the direction of their ground truth values. No general conclusion can be observed about the evolution of material parameters in function of the iteration number of the CMC fitting approach, although it is important to note that material parameters for the constrained mixture theory cannot simply be replaced by 390 classically obtained parameters.

4.2. Application to experimental data

After verifying the iterative CMC parameter fitting approach with numerically constructed test data, the approach was also tested with actual planar biaxial test data. A diastolic geometry was build in Abaqus, where the *in vivo*

395 thickness was determined based on trial-and-error. Better measurements of *in vivo* wall thicknesses should provide a solution.

The observed results of the CMC parameter fitting are in line with the previous results. The relative difference between initial and final parameters sets is comparable, such that the datasets used for verification seem representative
400 for real test data. The required number of iterations is similar as well.

From figure 6, it can be seen that parameter $C_{10,M}$ decreases, while k_1 increases. This shift of parameters most likely is a direct consequence of the shift in stretch state of both constituents due to the application of deposition stretches. It can be observed that after four iterations, the parameters no longer
405 change significantly. Therefore, the advantage of going through the last three iterations might not outweigh the higher computational cost, such that the convergence criterion may be made less strict, depending on the accuracy sought for.

4.3. Comparison of the classical and constrained mixture modeling approach

410 Figure 7 shows the model and experimental data. An offset from the zero force at stretch 1 can be observed. This is caused by a preload applied during the biaxial test to avoid sagging of the sample at the start, leading to a deviation to the model at low stresses. However, this artefact does not affect the aim of the present study to compare the classical parameter fitting approach with the new
415 CMC method. Nonetheless, further research, beyond the scope of the present study, is necessary to correct for it in an accurate and straightforward manner.

The model data obtained from the classical approach matches the experimental data slightly better than at the final fit, although the difference is minimal. It was observed that the final fit was sensitive to the value for $g_{e,ax}$ and that a
420 good choice is crucial to obtain a material model that matches the experiments. It was set to a realistic value of axial prestretch. However, no exact value for the specific sample was available. Also g_c affects the results. It was estimated at 1.1, corresponding to an approximate value found in mouse carotid arteries [28], which is possibly inaccurate for sheep pulmonary arteries. Performing

425 experimental tests on the stretch state of collagen would be beneficial for the
reliability.

Figure 8 shows the resulting stress states. Note that the sudden drop of stress
between media and adventitia arises from the difference in stiffness. It can be
observed that both models show very similar wall stresses. The circumferential
430 Cauchy stress in the medial layer is almost constant through the thickness. The
homogenization of the wall stress is even clearer in the results of the constrained
mixture model, showing its strength in representing residual stresses. Three
possible reasons for the small difference between both models are listed. Firstly,
this is partly due to a different fit of both models to the experimental data,
435 such that the stress-stretch response is not the same. A second reason is the
assumption of a stress-free radially cut state in the classical approach. From
the results of the FE model following the constrained mixture approach, it
can be seen that the stresses in the radially cut state are not exactly zero but
approximately two orders of magnitude smaller than at diastole. Thirdly, the
440 deformations from the diastolic state to the radially cut state, i.e. $\mathbf{F}_{release}$ and
 \mathbf{F}_{open} are approximated and averaged over the element layers when integrated in
the constrained mixture parameter fitting. On the other hand, no approximation
was needed going from the stress-free state to the diastolic state in the classical
FE model. A similarity between both modeling approaches is the fact that the
445 radially cut state is considered to match the planar state at the beginning of
the tensile test. In neither of the cases, a flattening deformation is considered.

Both modeling approaches yield similar results. Neither approach can be
easily validated due to the apparent lack of a ground truth material state. How-
ever, the constrained mixture approach offers the advantage that no stress-free
450 reference geometry is required. Therefore, it is preferred over the classical mod-
eling method.

4.4. Implications of results

Bellini *et al.* [28] developed an improved mechanical model for arterial tis-
sue based on histological and clinical data. It enables to capture the effects of

455 the residual stresses while considering a known *in vivo* reference state. Several studies have suggested, both experimentally and computationally, that this constrained mixture modeling approach reliably predicts residual stresses and the mechanical behavior of arterial tissue [28, 36, 40, 44]. Moreover, it provides an elegant framework for the growth and remodeling algorithms in soft tissues
460 that are microstructurally relevant. However, to our best knowledge, no such material parameters from planar biaxial tests have been obtained before.

The aim of the present study was to provide an alternative planar biaxial tensile parameter fitting method, hypothesizing that the constrained mixture approach requires an alternative set of material parameters because of a shift in
465 energy contribution of the different constituents due to their different deformation states. The results of the verification study show a clear difference between classical and CMC parameter sets, while figure 7 shows a similar fit of the experimental data. These findings are in agreement with those of Mousavi and Avril [40]. However, they found an increase in elastin stiffness and decrease in
470 collagen stiffness for the constrained mixture model. This cannot be generally concluded from the present results, presumably due to the following differences in research approach. First, they use a slightly different constitutive model, with four fiber families, where no fiber distribution is considered. Second, the present study uses biaxial tensile test data, as opposed to uniaxial test data in
475 multiple directions, possibly yielding a different constitutive behavior. In any case, given the clear difference, but unclear relation between the classical and CMC material parameter sets, the use of this developed iterative parameter fitting approach is of great importance to define a reliable constitutive model for arterial tissue based on the constrained mixture theory.

480 4.5. Limitations and future work

A number of limitations can be attributed to the presently defined parameter fitting approach. First, the constrained mixture model considers an *in vivo* reference state, such that all deformations with respect to that state need to be considered. However, one of these, i.e. between the radially cut configuration

485 and the flattened out test sample, is currently ignored, since its determination
from FE simulations is not straightforward. We assume this to be reasonable due
to small flattening stretches and negligible stresses that are often counteracted
by gravity in practice. A second limitation is related to g_c and $g_{e,ax}$. These
deposition stretches are assumed to be fixed and known. Unreported tests show
490 the sensitivity of the method to variations in these parameters, which is why
reliable deposition stretch values are deemed important. However, experimental
methods to determine them are scarce. To our knowledge, only Bellini *et al.* [28]
have reported a value for g_c . They refer to Ferruzzi *et al.* [45], who were able
to experimentally distinguish the stress-free state of collagen from the unloaded
495 arterial configuration. Bellini *et al.* fine-tuned these approximate values by
optimizing the fit of model data to experimental data. The parameter g_{ax} is
closely related to the overall axial prestretch that can be measured upon excision
of an artery. If necessary, g_c and $g_{e,ax}$ can be considered as extra parameters to
be fitted. In that case, overparameterization may be avoided by obtaining the
500 fiber angles and dispersion from histological data, such that no more than five
parameters need to be fitted.

The method was verified by the numerical construction of mechanical test
data, obtained from the FE simulation of an ideal planar biaxial test. It must
be noted that this approach is only valid if the chosen constitutive behavior is
505 a good description of the behavior of arterial tissue. The transverse behavior
of the GOH model has been found to be unrealistic [46, 47]. Moreover, the
implemented tension-compression switch has been criticised earlier [48], such
that improved material models must be considered. Also the choice of param-
eter dependence between the medial and adventitial layer might be unrealistic.
510 Nevertheless, we hypothesize that the proposed parameter fitting method is
independent of the chosen material model. The parameter dependencies were
chosen based on approximate elastic versus fiber content in both layers and help
to reduce the number of parameters to be fitted.

The constrained mixture model is microstructurally motivated [28] and a
515 good prediction of the mechanical behavior of arterial tissue has been shown

[40], such that it is assumed to be valid in the present study. However, an idealized planar biaxial test yields a uniform stress state per material layer, unattainable during an actual test. Inhomogeneities arise from nonideal boundary conditions. This impedes the obtention of the correct material parameters
520 as compared to the ideal situation. Fehervary *et al.* [49] proposed an alternative parameter fitting approach to handle these inhomogeneities. Future work should be directed at integrating this approach with the currently proposed approach.

The current approach assumes an ideal cylindrical geometry and a resulting homogeneous stress state per element layer. No regional diameter, thickness,
525 or material variations are taken into account. Future work will be directed towards nonideal geometries, where a patch of material will be virtually cut out of a patient-specific geometry.

5. Conclusion

The constrained mixture theory for the modeling of the arterial wall consid-
530 ers constituent-specific deformations and an *in vivo* reference state. We assume that this approach requires different material parameters. A framework for an iterative method to obtain these parameters based on planar biaxial test data was introduced, verified and tested. This study showed that the iterative fitting approach reliably converges towards the desired CMC material parameters. It
535 can also be seen that, for specific test data sets, these parameters must be distinguished from classically obtained material parameters. Indeed, both fitting approaches yield different material parameters, such that FE models following the classical or the constrained mixture modeling theory require an adequate set of material parameters. In a first application of the iterative fitting method
540 to actual experimental data, clear convergence occurs towards a set of CMC material parameters. These parameters, used in a FE model based on the constrained mixture approach are an important step towards patient-specific modeling of arteries, as well as reliable growth and remodeling algorithms.

Acknowledgements.

545

This work was supported by a doctoral grant strategic basic research (SB 1S35316N) to JV, a doctoral fellowship (11A6519N) to LM and a postdoctoral fellowship (PDO/012) to NF of the Research Foundation-Flanders (FWO). Support was also provided by KU Leuven through a category 2 research project
550 (C2-ADAPT). SA is grateful to ERC for the ERC-2014-CoG BIOLOCHANICS grant.

Appendix A: Implementation of the algorithm to find elastin deposition stretches

The iterative finite element method, described in section 2.2 of the manuscript,
555 is constructed as follows. In a first step, an arterial geometry is pressurized. In all following steps, the applied pressure is kept constant, while the stretch state of the material is updated until the geometry has returned to its original shape. At each simulation step, a UMAT subroutine is called in which the elastin deposition stretch tensor is updated. This tensor \mathbf{G}_e is stored in state dependent
560 variables (STATEV). This subroutine provides the current deformation gradient and requires a resulting Cauchy stress (STRESS) and a Jacobian Matrix (DDSDDE).

At the end of each step, a URDFIL subroutine is called. Within URDFIL, the utility routine POSFIL is called to read from the results file with DBFILE.
565 This allows to store the present deformation gradient in a global variable \mathbf{F}_{dep} and to stop the simulation when convergence has been reached.

call user subroutine UMAT:

if STEP==1

570 STATEV = $\mathbf{G}_{e,initial}$ (see equation 7)

endif

```

Ge = STATEV

575 if STEP > 1
      Ge = FdepGe
      STATEV = Ge
    endif

580 Gc = Gc(gc, M) (see equation 6)
    σij = 1/J ∂Ψ(F, Ge, Gc) / ∂Fia Fja (see equation 13)
    Cijkl = σijδkl + 1/2 ( ∂σij / ∂Fka Fla + ∂σij / ∂Fla Fka )
    (see Nolan et al. [50], where C represents the Consistent Tangent Matrix and
    δkl is the Kronecker delta)

585
    STRESS = σ (convert 3x3 tensor to 6x1)
    DDSDD = C (convert 3x3x3x3 tensor to 6x6)

    call user subroutine URDFIL:

590 call POSFIL:
    call DBFILE:

    read F from results file (deformation gradient)
    Fdep = F

595
    read U11, U22, U33 from results file (nodal displacement)
    Uav = ∑n √(U11,n + U22,n + U33,n) (average nodal displacement over all nodes n)

    if Uav < Tol (Tol set to 1% of the wall thickness)

600      STOP simulation
    endif

```

References

- [1] P. Dobrin, T. Canfield, S. Sinha, Development of longitudinal retraction of carotid arteries in neonatal dogs, *Experientia* 31 (11) (1975) 1295–1296. doi:10.1007/BF01945788. 605
- [2] D. H. Bergel, Viscoelastic properties of the arterial wall, Ph.D. thesis (1960).
- [3] R. N. Vaishnav, J. Vossoughi, Estimation of residual strains in aortic segments, in: *Biomedical Engineering II: Recent Developments*, 1983, pp. 330–333. doi:10.1016/B978-0-08-030145-7.50078-7. 610
- [4] C. J. Chuong, Y. C. Fung, Three-dimensional stress distribution in arteries., *J Biomech Eng-T ASME* 105 (3) (1983) 268–274. doi:10.1115/1.3138417.
- [5] C. J. Chuong, Y. C. Fung, On residual stresses in arteries., *Journal of biomechanical engineering* 108 (2) (1986) 189–92. 615
URL <http://www.ncbi.nlm.nih.gov/pubmed/3079517>
- [6] A. Rachev, S. Greenwald, Residual strains in conduit arteries, *Journal of Biomechanics* 36 (5) (2003) 661–670. doi:10.1016/S0021-9290(02)00444-X.
- [7] S. Q. Liu, Y. C. Fung, Relationship between hypertension, hypertrophy, and opening angle of zero-stress state of arteries following aortic constriction., *Journal of biomechanical engineering* 111 (4) (1989) 325–335. doi:10.1115/1.3168386. 620
- [8] R. N. Vaishnav, J. Vossoughi, Residual stress and strain in aortic segments, *Journal of Biomechanics* 20 (3). doi:10.1016/0021-9290(87)90290-9.
- [9] M. K. Hong, J. Vossoughi, C. C. Haudenschild, S. C. Wong, B. D. Zuckerman, M. B. Leon, Vascular effects of diet-induced hypercalcemia after balloon artery injury in giant Flemish rabbits, *American Heart Journal* 130 (4) (1995) 758–764. doi:10.1016/0002-8703(95)90074-8. 625

- [10] T. Matsumoto, K. Hayashi, K. Ide, Residual strain and local strain distributions in the rabbit atherosclerotic aorta, *Journal of Biomechanics* 28 (10) (1995) 1207–1217. doi:10.1016/0021-9290(94)00179-8.
- [11] J. Vossoughi, H. Hedjazi, F. Borris, Intimal residual stress and strain in large arteries, in: *ASME Bioengineering Conference*, New York, 1993, pp. 434–437.
- [12] L. A. Taber, D. W. Eggers, Theoretical study of stress-modulated growth in the aorta, *Journal of Theoretical Biology* 180 (4) (1996) 343–357. doi:10.1006/jtbi.1996.0107.
- [13] G. A. Holzapfel, T. C. Gasser, R. W. Ogden, A new constitutive framework for arterial wall mechanics and a comparative study of material models, *Journal of Elasticity* 61 (1-3) (2000) 1–48. arXiv:A:1010835316564, doi:10.1023/A:1010835316564.
- [14] L. A. Taber, J. D. Humphrey, Stress-Modulated Growth, Residual Stress, and Vascular Heterogeneity, *Journal of Biomechanical Engineering* 123 (6) (2001) 528. doi:10.1115/1.1412451.
URL <http://biomechanical.asmedigitalcollection.asme.org/article.aspx?articleid=1476131>
- [15] T. C. Gasser, C. J. Schulze-Bauer, G. Holzapfel, A Three-dimensional Finite Element Model for Arterial Clamping, *Journal of Biomechanical Engineering* 124 (4) (2002) 355. doi:10.1115/1.1485284.
URL <http://link.aip.org/link/JBENDY/v124/i4/p355/s1{&}Agg=doi>
- [16] M. L. Raghavan, S. Trivedi, A. Nagaraj, D. D. McPherson, K. B. Chandran, Three-dimensional finite element analysis of residual stress in arteries, *Annals of Biomedical Engineering* 32 (2) (2004) 257–263. doi:10.1023/B:ABME.0000012745.05794.32.
- [17] D. Balzani, J. Schröder, D. Gross, Numerical simulation of residual stresses

in arterial walls, *Computational Materials Science* 39 (1 SPEC. ISS.) (2007) 117–123. doi:10.1016/j.commatsci.2005.11.014.

- [18] N. Famaey, G. Sommer, J. Vander Sloten, G. A. Holzapfel, Arterial clamping: finite element simulation and in vivo validation., *Journal of the Mechanical Behavior of Biomedical Materials* 12 (2012) 107–118. doi:10.1016/j.jmbbm.2012.03.010.
660 URL <http://dx.doi.org/10.1016/j.jmbbm.2012.03.010>
- [19] S. de Putter, B. J. Wolters, M. C. Rutten, M. Breeuwer, F. A. Gerritsen, F. N. van de Vosse, Patient-specific initial wall stress in abdominal aortic aneurysms with a backward incremental method, *Journal of Biomechanics* 40 (5) (2007) 1081–1090. doi:10.1016/j.jbiomech.2006.04.019.
665
- [20] H. Weisbecker, D. M. Pierce, G. A. Holzapfel, A generalized prestressing algorithm for finite element simulations of preloaded geometries with application to the aorta, *International Journal for Numerical Methods in Biomedical Engineering* 30 (9) (2014) 857–872. arXiv:NIHMS150003, doi:10.1002/cnm.2632.
670
- [21] J. Bols, J. Degroote, B. Trachet, B. Verhegghe, P. Segers, J. Vierendeels, A computational method to assess the in vivo stresses and unloaded configuration of patient-specific blood vessels, *Journal of Computational and Applied Mathematics* 246 (2013) 10–17. doi:10.1016/j.cam.2012.10.034.
675
- [22] M. L. Raghavan, B. Ma, M. F. Fillinger, Non-invasive determination of zero-pressure geometry of arterial aneurysms, *Annals of Biomedical Engineering* 34 (9) (2006) 1414–1419. doi:10.1007/s10439-006-9115-7.
- [23] M. W. Gee, C. Reeps, H. H. Eckstein, W. A. Wall, Prestressing in finite deformation abdominal aortic aneurysm simulation, *Journal of Biomechanics* 42 (11) (2009) 1732–1739. doi:10.1016/j.jbiomech.2009.04.016.
680
- [24] M. W. Gee, C. Förster, W. A. Wall, A computational strategy for prestressing patient-specific biomechanical problems under finite deformation,

- International Journal for Numerical Methods in Biomedical Engineering
685 26 (1) (2010) 52–72. [arXiv:NIHMS150003](#), [doi:10.1002/cnm.1236](#).
- [25] Y. C. Fung, What are the residual stresses doing in our blood vessels?,
Annals of Biomedical Engineering 19 (3) (1991) 237–249. [doi:10.1007/BF02584301](#).
- [26] P. J. Zeller, T. C. Skalak, Contribution of individual structural components
690 in determining the zero-stress state in small arteries, Journal of Vascular
Research 35 (1) (1998) 8–17. [doi:10.1159/000025560](#).
- [27] E. C. Davis, Elastic lamina growth in the developing mouse aorta., The
journal of histochemistry and cytochemistry : official journal of the Histo-
chemistry Society 43 (11) (1995) 1115–23. [doi:10.1177/43.11.7560894](#).
695 URL <http://www.ncbi.nlm.nih.gov/pubmed/7560894>
- [28] C. Bellini, J. Ferruzzi, S. Roccabianca, E. S. Di Martino, J. D. Humphrey,
A Microstructurally Motivated Model of Arterial Wall Mechanics with
Mechanobiological Implications, Annals of Biomedical Engineering 42 (3)
(2014) 488–502. [doi:10.1007/s10439-013-0928-x](#).
700 URL <http://link.springer.com/10.1007/s10439-013-0928-x>
- [29] J. D. Humphrey, K. R. Rajagopal, A Constrained Mixture Model For
Growth And Remodelling Of Soft Tissues, Mathematical Models and
Methods in Applied Sciences 12 (03) (2002) 407–430. [arXiv:0036013702](#),
[doi:10.1142/S0218202502001714](#).
705 URL <http://www.worldscientific.com/doi/abs/10.1142/S0218202502001714>
- [30] N. Famaey, J. Vastmans, H. Fehervary, L. Maes, E. Vanderveken, F. Rega,
S. J. Mousavi, S. Avril, Numerical simulation of arterial remodeling in
pulmonary autografts, ZAMM - Journal of Applied Mathematics and Me-
chanics / Zeitschrift für Angewandte Mathematik und Mechanik 98 (12)
710 (2018) 2239–2257. [doi:10.1002/zamm.201700351](#).
URL <http://doi.wiley.com/10.1002/zamm.201700351>

- [31] F. A. Braeu, A. Seitz, R. C. Aydin, C. J. Cyron, Homogenized constrained mixture models for anisotropic volumetric growth and remodeling, *Biomechanics and Modeling in Mechanobiology* doi:10.1007/s10237-016-0859-1. 715
- [32] C. J. Cyron, R. C. Aydin, J. D. Humphrey, A homogenized constrained mixture (and mechanical analog) model for growth and remodeling of soft tissue, *Biomechanics and Modeling in Mechanobiology* (2016) 1–15 doi:10.1007/s10237-016-0770-9. 720
- [33] P. N. Watton, N. A. Hill, Evolving mechanical properties of a model of abdominal aortic aneurysm, *Biomechanics and Modeling in Mechanobiology* doi:10.1007/s10237-007-0115-9.
- [34] S. Zeinali-Davarani, S. Baek, Medical image-based simulation of abdominal aortic aneurysm growth, *Mechanics Research Communications* doi:10.1016/j.mechrescom.2012.01.008. 725
- [35] S. Baek, K. R. Rajagopal, J. D. Humphrey, A Theoretical Model of Enlarging Intracranial Fusiform Aneurysms, *Journal of Biomechanical Engineering* arXiv:33645723580, doi:10.1115/1.2132374.
- [36] A. Valentín, J. D. Humphrey, G. A. Holzapfel, A finite element-based constrained mixture implementation for arterial growth, remodeling, and adaptation: Theory and numerical verification, *International Journal for Numerical Methods in Biomedical Engineering* 29 (8) (2013) 822–849. arXiv:NIHMS150003, doi:10.1002/cnm.2555. 730
- [37] C. Alberto Figueroa, S. Baek, C. A. Taylor, J. D. Humphrey, A computational framework for fluid-solid-growth modeling in cardiovascular simulations, *Computer Methods in Applied Mechanics and Engineering* doi:10.1016/j.cma.2008.09.013. 735
- [38] T. C. Gasser, R. W. Ogden, G. A. Holzapfel, Hyperelastic modelling of arterial layers with distributed collagen fibre orientations, *Journal of The* 740

Royal Society Interface 3 (6) (2006) 15–35. doi:10.1098/rsif.2005.0073.

URL <http://linkinghub.elsevier.com/retrieve/pii/S1751616112000902><http://rsif.royalsocietypublishing.org/cgi/doi/10.1098/rsif.2005.0073>

745 [39] H. Weisbecker, D. M. Pierce, P. Regitnig, G. A. Holzapfel, Layer-specific damage experiments and modeling of human thoracic and abdominal aortas with non-atherosclerotic intimal thickening, *Journal of the Mechanical Behavior of Biomedical Materials* 12 (2012) 93–106. doi:10.1016/j.jmbbm.2012.03.012.

750 [40] S. J. Mousavi, S. Avril, Patient-specific stress analyses in the ascending thoracic aorta using a finite-element implementation of the constrained mixture theory, *Biomechanics and Modeling in Mechanobiology* 16 (5) (2017) 1765–1777. doi:10.1007/s10237-017-0918-2.

[41] J. Vastmans, H. Fehervary, P. Verbrugghe, T. Verbelen, E. Vanderveken, 755 J. Vander Sloten, T. Treasure, F. Rega, N. Famaey, Biomechanical evaluation of a personalized external aortic root support applied in the Ross procedure, *Journal of the Mechanical Behavior of Biomedical Materials* 78 (2018) 164–174. doi:10.1016/j.jmbbm.2017.11.018.

[42] E. Vanderveken, J. Vastmans, T. Verbelen, P. Verbrugghe, N. Famaey, 760 E. Verbeken, T. Treasure, F. Rega, Reinforcing the pulmonary artery autograft in the aortic position with a textile mesh: a histological evaluation, *Interactive CardioVascular and Thoracic Surgery* 27 (4) (2018) 566–573. doi:10.1093/icvts/ivy134.

URL <http://www.ncbi.nlm.nih.gov/pubmed/29912400><https://academic.oup.com/icvts/article/27/4/566/4975496>

[43] V. Pratt, Direct least-squares fitting of algebraic surfaces, *ACM SIGGRAPH Computer Graphics* 21 (4) (1987) 145–152. doi:10.1145/37402.37420.

URL <http://portal.acm.org/citation.cfm?doid=37402.37420>

- 770 [44] L. Cardamone, A. Valentín, J. F. Eberth, J. D. Humphrey, Origin of axial prestretch and residual stress in arteries, *Biomechanics and Modeling in Mechanobiology* 8 (6) (2009) 431–446. [arXiv:NIHMS150003](https://arxiv.org/abs/NIHMS150003), [doi:10.1007/s10237-008-0146-x](https://doi.org/10.1007/s10237-008-0146-x).
- [45] J. Ferruzzi, M. J. Collins, A. T. Yeh, J. D. Humphrey, Mechanical assess-
775 ment of elastin integrity in fibrillin-1-deficient carotid arteries: Implications for Marfan syndrome, *Cardiovascular Research* [doi:10.1093/cvr/cvr195](https://doi.org/10.1093/cvr/cvr195).
- [46] P. Skacel, J. Bursa, Poisson's ratio of arterial wall - Inconsistency of constitutive models with experimental data, *Journal of the Mechanical Behavior of Biomedical Materials* [doi:10.1016/j.jmbbm.2015.09.029](https://doi.org/10.1016/j.jmbbm.2015.09.029).
- 780 [47] M. Latorre, X. Romero, F. J. Montáns, The relevance of transverse deformation effects in modeling soft biological tissues, *International Journal of Solids and Structures* [doi:10.1016/j.ijsolstr.2016.08.006](https://doi.org/10.1016/j.ijsolstr.2016.08.006).
- [48] G. A. Holzapfel, R. W. Ogden, On the tension-compression switch in soft fibrous solids, *European Journal of Mechanics, A/Solids* [doi:10.1016/j.
785 euromechsol.2014.09.005](https://doi.org/10.1016/j.euromechsol.2014.09.005).
- [49] H. Fehervary, M. Smoljkić, J. Vander Sloten, N. Famaey, Planar biaxial testing of soft biological tissue using rakes: A critical analysis of protocol and fitting process, *Journal of the Mechanical Behavior of Biomedical Materials* 61 (2016) 135–151. [doi:10.1016/j.jmbbm.2016.01.011](https://doi.org/10.1016/j.jmbbm.2016.01.011).
790 URL www.elsevier.com/locate/jmbbmwww.sciencedirect.com<http://dx.doi.org/10.1016/j.jmbbm.2016.01.011>
- [50] D. R. Nolan, A. L. Gower, M. Destrade, R. W. Ogden, J. P. McGarry, A robust anisotropic hyperelastic formulation for the modelling of soft tissue, *Journal of the Mechanical Behavior of Biomedical Materials* 39 (2014) 48–
795 60. [doi:10.1016/j.jmbbm.2014.06.016](https://doi.org/10.1016/j.jmbbm.2014.06.016).